White top-emitting organic light-emitting diodes with solution-processed nano-particle scattering layers

Tim Schaefer, Tobias Schwab, Simone Lenk, and Malte C. Gather

Citation: Applied Physics Letters **107**, 233301 (2015); doi: 10.1063/1.4937004

View online: http://dx.doi.org/10.1063/1.4937004

View Table of Contents: http://scitation.aip.org/content/aip/journal/apl/107/23?ver=pdfcov

Published by the AIP Publishing

White top-emitting organic light-emitting diodes with solution-processed nano-particle scattering layers

Tim Schaefer,[1,2] Tobias Schwab,[1] Simone Lenk,[1] and Malte C. Gather[1,3,a)]
[1]*Institut für Angewandte Photophysik, Technische Universität Dresden, 01062 Dresden, Germany*
[2]*Institut für Physikalische Chemie, Universität zu Köln, 50939 Köln, Germany*
[3]*Organic Semiconductor Centre, SUPA, School of Physics and Astronomy, University of St Andrews, St Andrews KY16 9SS, Scotland, United Kingdom*

(Received 6 July 2015; accepted 22 November 2015; published online 7 December 2015)

A random scattering approach to enhance light extraction in white top-emitting organic light-emitting diodes (OLEDs) is reported. Through solution processing from fluorinated solvents, a nano-particle scattering layer (NPSL) can be deposited directly on top of small molecule OLEDs without affecting their electrical performance. The scattering length for light inside the NPSL is determined from transmission measurements and found to be in agreement with Mie scattering theory. Furthermore, the dependence of the light outcoupling enhancement on electron transport layer thickness is studied. Depending on the electron transport layer thickness, the NPSL enhances the external quantum efficiency of the investigated white OLEDs by between 1.5 and 2.3-fold. For a device structure that has been optimized prior to application of the NPSL, the maximum external quantum efficiency is improved from 4.7% to 7.4% (1.6-fold improvement). In addition, the scattering layer strongly reduces the undesired shift in emission color with viewing angle. [http://dx.doi.org/10.1063/1.4937004]

White organic light-emitting diodes (OLEDs) are promising candidates for future applications in lighting and provide homogenous and glare-free illumination over a large area. They enable flexible applications and have the potential for low-cost manufacturing. Even though their internal quantum efficiencies can be near 100%, the external quantum efficiency (EQE) of conventional OLEDs is fundamentally limited to 20%–30% (with the actual value depending on several factors including whether emitter molecules are oriented isotropically or not),[1–3] due to total internal reflection (TIR) caused by the refractive index mismatch between the organic materials and the surrounding air. Therefore, a number of light outcoupling strategies, including high refractive index glass,[4] microlens arrays,[5] low-index grids,[6] or scattering layers,[7] have been investigated. These systems can be easily applied to the glass substrate of common bottom-emitting OLEDs in which light is extracted through the device substrate. In contrast, for top-emitting OLEDs, only two main outcoupling approaches exist: (i) introducing a non-planar light-scattering structure beneath the OLED[8] or (ii) adding a light-scattering structure on top of the device.[9] Whilst the latter approach would in principle be preferable, deposition of suitable structures on top of a functional OLED has proven to be tremendously challenging because deposition of the outcoupling structure tends to damage the OLED. Furthermore, restrictions due to encapsulation need to be considered.

For top-emitting OLEDs, an organic capping layer is typically evaporated on top of the device. This enhances light outcoupling to some extent, even though it does not completely solve the problem of TIR.[10–12] Thomschke *et al*.[13] demonstrated the lamination of a high refractive index microlens foil on top of a white OLED and obtained a device efficacy of over 30 lm/W (27% EQE). Recently, Kim *et al*. achieved an EQE of 44.7% (1.8-fold enhancement) for a green top-emitting OLED using a microlens array that was fabricated by evaporating an organic capping layer through a shadow mask.[14] An overview of currently known outcoupling approaches for both bottom and top emitting white OLEDs is given in Refs. 15 and 16.

Here, we propose a different approach to enhance outcoupling in top-emitting white OLEDs with a random scattering layer that is located directly on top of the OLED stack. Our method allows us to deposit from solution a nano-particle scattering layer (NPSL) on top of white OLEDs without damaging the device underneath. The use of random scattering layers is advantageous as it enables uniform emission in terms of spectra and angular dependent radiation pattern. Moreover, adjusting particle size, concentration, and layer thickness allows for easy optimization of the system. We study the outcoupling enhancement of the NPSL as a function of the electron transport layer (ETL) thickness of white top-emitting OLEDs. As the ETL thickness strongly affects the tuning of the optical microcavity formed by the OLED and thus the optical efficiency of the structure, it is important to vary this parameter when studying new light extraction techniques.

To deposit our NSPL from solution without inducing damage to the OLED stack underneath, we rely on a combination of a fluorinated polymer matrix loaded with titanium dioxide (TiO_2) nano-particles and a hydrofluoroether (HFE) solvent. HFEs have previously been used as orthogonal solvents for photolithographic patterning of organic films.[17–20] As orthogonal solvents, they are chemically benign to most organic materials and do not dissolve films of organic materials.[21] HFEs are also used as solvents for fluorinated

a)mcg6@st-andrews.ac.uk

polymer photoresists.[22,23] Recently, micro-patterning of highly efficient OLEDs using HFE as developer has been demonstrated.[24]

The organic and metal layers of our white OLEDs were thermally evaporated in a vacuum chamber (Kurt J. Lesker) at a base pressure of about 10^{-8} mbar. OLED stacks were deposited on individual glass substrates (thickness 1.1 mm, Corning Eagle XG, Thin Film Devices, Inc.). The layer sequence is as follows (from bottom to top): glass substrate/40 nm Al/40 nm Ag/20 nm 2,2′,7,7′-tetrakis-(*N*,*N*-di-methyl-phenylamino)–9,9′-spiro-bifluorene (Spiro-TTB): 2,2′-(perfluoronaphthalene-2,6-diylidene)dimalononitrile (F6-TCNNQ, 4 wt. %)/10 nm 4,40-bis[*N*-(1-naphthyl)-*N*-phenylamino] biphenyl (NPB)/10 nm NPB:Iridium(III)bis(2-methyl-dibenzo[f,h]quinoxaline)(acetylacetonate) ($Ir(MDQ)_2(acac)$) (5 wt. %)/3 nm 4,4′,4″tris(*N*-carbazolyl)-triphenylamine (TCTA):tris(2-phenylpyridine)iridium(III) ($Ir(ppy)_3$) (5 wt. %)/2 nm TCTA:2,2′,2″-(1,3,5-phenylen)tris(1-phenyl-1H-benzimidazole) (TPBI, 1:2)/10 nm 2-methyl-9,10-bis (naphthalen-2-yl)anthracene (MADN):2,5,8,11-tetra-tert-butylperylene (TBPe, 1 wt. %)/10 nm 4,7-diphenyl-1,10-phenan-throlin (BPhen)/80–125 nm BPhen:Cs (1:1)/2 nm Au/9 nm Ag/50 nm NPB. The transparent thin metal cathode is based on the wetting layer concept.[25] The devices have an active area of 6.76 mm^2. The OLED layer architecture used in this study is illustrated in Figure 1(a). All OLEDs were processed in the same evaporation run, varying the thickness of the ETL between 80 and 125 nm for the different devices. For the NPSL, TiO_2 nano-particles (rutile, mean diameter 250 nm, mkNANO) were dispersed in a solution of fluorinated photoresist (OSCoR 4000, Orthogonal, Inc.) at a concentration of 50 g/l by shaking and ultrasound treatment. NPSLs were fabricated by dip-coating complete OLEDs (Figure 1(b)) into the nano-particle loaded resist solution. Dip-coating was performed at a pull-out speed of 0.2 mm/s with the dip-coater located in a nitrogen filled glovebox with an organic solvent removal filter. For our device layout, four identical OLEDs are processed on each substrate. By dip-coating only the lower half of the sample, we obtain two coated and two uncoated OLEDs (references) next to each other and can thus ensure good comparability. The HFE solvent of the resist evaporates at room temperature, forming a layer of TiO_2 nanoparticles embedded within a fluorinated polymer matrix. The particle density in the final film is about 8 particles per μm^3. Pristine, glass substrates without an OLED stack were dip-coated simultaneously to determine the optical properties and the thickness of the formed NPSLs. (According to profilometer measurements, the thickness of NPSLs deposited on blank glass substrates and on OLED stacks did not differ.) After dip-coating, the OLEDs were encapsulated under nitrogen atmosphere using cavity glass lids. Current-voltage characteristics and electroluminescence spectra are taken using an automated measurement setup with a source measurement unit and a calibrated CAS140CT spectrometer (Instrument Systems GmbH). Angular-dependent spectra are measured in 5° steps with a custom-made spectro-goniometer comprising a fiber coupled Ocean Optics USB 4000 spectrometer. A photograph of the complete OLED with one pixel operating is shown in Figure 1(c). Simple optical characterization of the NPSL is performed with a light microscope (JENAVAL, Carl

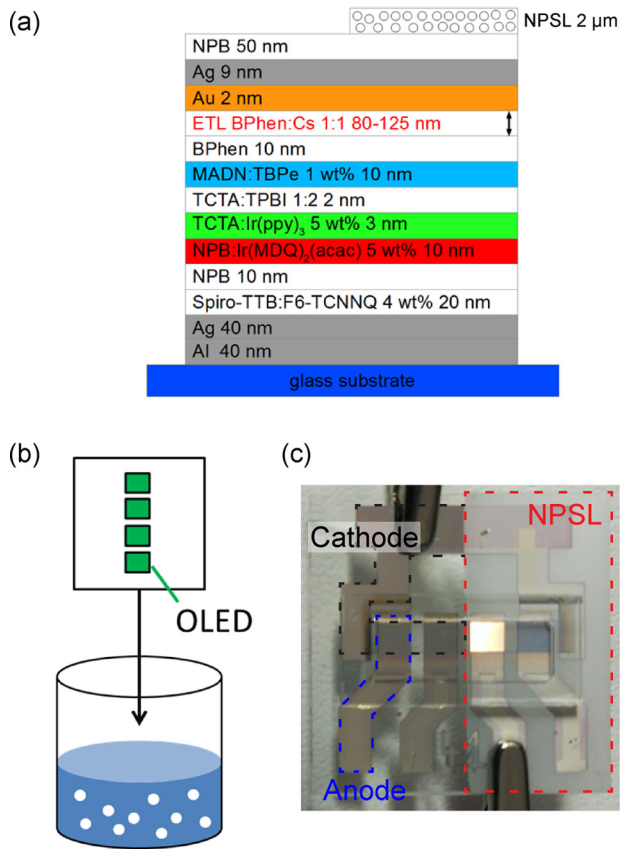

FIG. 1. (a) Layer architecture of the OLED series under investigation. Reference devices feature no NPSL on top. (b) Fabrication of the NPSL layer by dip-coating. TiO_2 nano-particles are dispersed in a solution of fluorinated photoresist by shaking and ultrasonic treatment and OLEDs are then dipped into the solution and pulled out slowly, depositing a homogenous NPSL on top of the OLED. (c) Photograph of complete OLED with NPSL deposited on the right half of the substrate. The area of the anode and the cathode is marked in the picture, but for clarity, labels are omitted on the NPSL covered half of the device. The second pixel from the right is operated, emitting warm white light.

Zeiss, Jena). To reveal the presence of any clusters, especially in dense, scattering layers, all samples are illuminated in transmission. The transmittance of the NPSLs is measured with a two-beam spectrophotometer (MPC-3100, Shimadzu). The NPSL thickness is determined with a profilometer (Dektak 150, Veeco).

Due to the large refractive index contrast between the fluorinated photoresist ($n = 1.44$) and TiO_2 ($n \approx 2.3$), efficient and homogeneous scattering across the entire visible part of the spectrum is expected. We quantify the scattering behavior of our films using two different transmission spectra from which we then calculate the "haze" of our samples. While the total transmittance T_{total} is measured with an integrating sphere to collect transmitted light over all angles, the direct transmittance T_{direct} is the transmittance measured in normal direction (within a 5° collection window). The haze is then defined as

$$haze = \frac{T_{total} - T_{direct}}{T_{total}}. \quad (1)$$

Figure 2(a) shows the total, direct, and haze spectrum of our NPSL. The average haze is 75%, and the total transmittance is 63% in the wavelength range of 430–780 nm. The

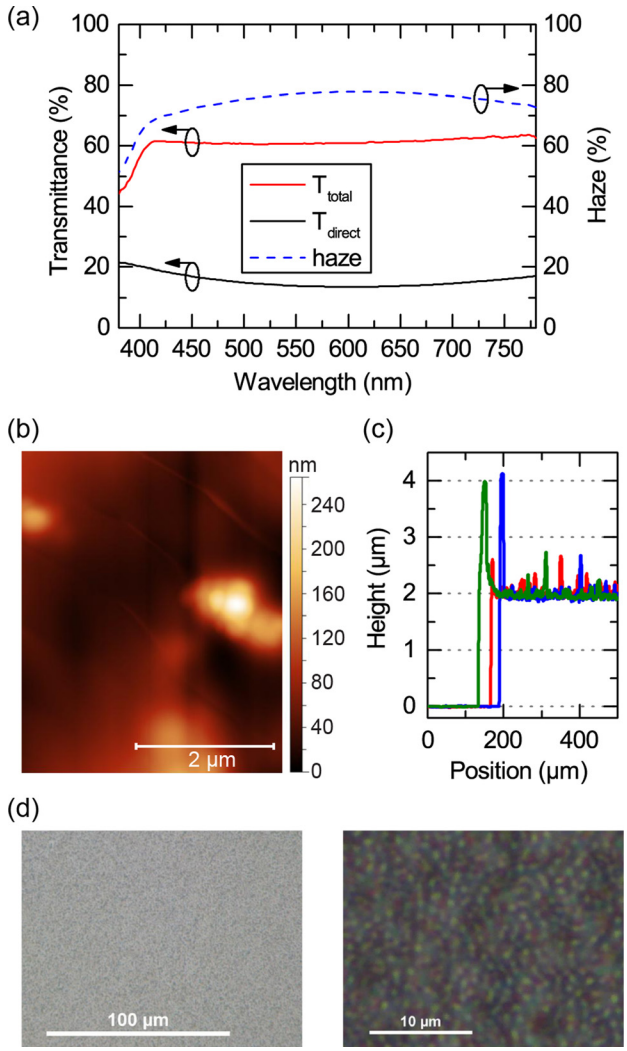

FIG. 2. (a) Optical properties of the NPSL measured on a glass substrate: total transmittance, direct transmittance, and haze. (b) Atomic force microscopy image showing the surface topography of a section of the NPSL surface. (c) Profilometer measurements across an edge of three NPSLs produced in two different batches. (d) Light microscope images of NPSL on glass at two different magnifications.

scattering coefficient μ_s can be calculated from this as $\mu_s = d^{-1}[\ln(T_{total,\mathrm{glass}}) - \ln(T_{direct,\mathrm{NPSL}})] = 0.98\,\mu\mathrm{m}^{-1}$ (where d is the NPSL thickness).[7] This value agrees well with Mie scattering theory:[26] Assuming spherical, non-absorbing, 250 nm-diameter TiO_2 particles embedded in an optically isotropic matrix, we obtain a scattering coefficient of $0.93\,\mu\mathrm{m}^{-1}$ and a scattering cross-section of $0.11\,\mu\mathrm{m}^2$. This supports that the majority of particles are well dispersed within the polymer matrix and contribute to scattering. Transmittance and haze were well reproduced between coating runs. (Supplementary Fig. S1 shows the optical characteristics of the first and last NPSLs produced when fabricating a batch of devices.[27])

Figure 2(b) shows an atomic force microscopy image of the NPSL surface topography. Single particles stand out of a smooth layer underneath. This is further evidence that nanoparticles are mostly embedded in the polymer matrix and implies that any outcoupling enhancement in OLEDs coated with NPSLs originates predominantly from internal rather than from surface scattering. Profilometer measurements show that NPSLs have an average thickness of 2 μm and a surfaces roughness (root-mean-square) of about 100 nm, with the thickness not changing significantly during fabrication of a batch of NPSL or between batches (Figure 2(c)). At larger length scales, the NPSLs are homogenous as can be seen in the light microscope images in Figure 2(d).

Current density-voltage characteristics of OLEDs with and without scattering layer are shown in Figure 3(a) (ETL thickness 80 nm). The OLED with the scattering layer exhibits slightly larger leakage current (a trend that is also observed for other samples, see supplementary Fig. S2).[27] We attribute this to the presence of impurities in the

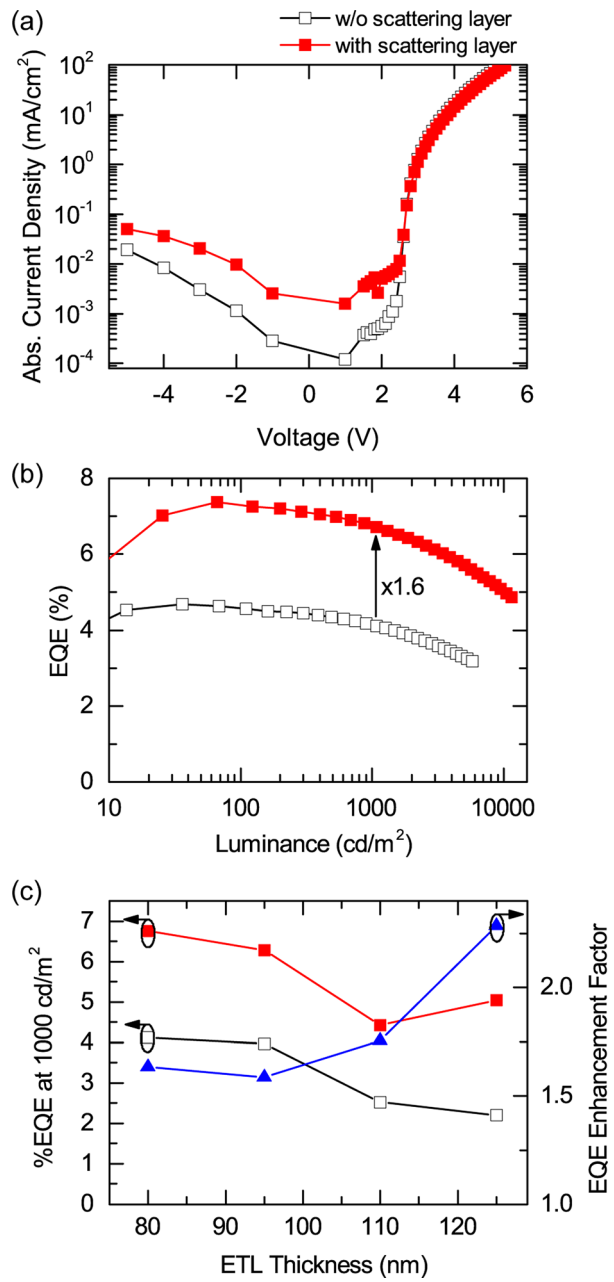

FIG. 3. (a) Current density-voltage characteristics and (b) external quantum efficiency versus luminance of white top-emitting OLEDs with an 80 nm thick electron transport layer, both with (red solid squares) and without (black open squares) NPSL. (c) External quantum efficiency at 1000 cd m^{-2} versus ETL thickness for devices with (red solid squares) and without scattering (black open squares) layer. Corresponding EQE enhancement factors are represented as blue triangles. Lines are guides to the eye.

photoresist solution, which penetrate into the organic stack during dip-coating. However, at operating voltage, the difference in current is negligible, which implies that the dip-coating process does not induce significant damage to the OLED stack underneath. Differences in EQE between NPSL containing devices and reference devices can consequently be attributed to changes in light outcoupling and are not an artifact related to changes of the electronic device properties. The EQE versus luminance characteristics indicate a maximum EQE of 7.4% for the OLED with and of 4.7% for the OLED without a scattering layer (Figure 3(b)). The latter value is within the expected range for a hybrid white top-emitting OLED using a second order cavity.[28] (As this paper focuses on outcoupling enhancement, the absolute EQE of the reference device is of minor importance.) At a luminance of 1000 cd m^{-2}, the EQE of the device with NPSL is 1.6 fold higher than the EQE of the reference.

Figure 3(c) shows the EQE and the EQE enhancement factor for a series of devices with different ETL thicknesses. For ETL thicknesses larger than 80 nm, the EQE drops for both device configurations. This is attributed to optical detuning of the top-emitting OLED cavity, i.e., the emitting layers are moved away from the maximum of the electromagnetic field for the corresponding wavelengths.[29] The EQE enhancement factor increases with ETL thickness, from about 1.6 for ETL thicknesses of 80 and 95 nm to 2.3 for an ETL thickness of 125 nm. We attribute this to the fact that for the 125 nm-OLED a significant fraction of the generated light is coupled to waveguided modes which limits the efficiency of the reference device. The large enhancement factor for the NSPL device with this ETL thickness indicates that the scattering layer is efficient at extracting light from these waveguided modes.

Figure 4(a) shows the total spectral irradiance of the different white top-emitting OLEDs, i.e., the spectral irradiance integrated over emission angles from 0° to 75°. Angle resolved emission spectra are shown in supplementary Fig. S3.[27] The ratio of the total spectral irradiance of devices with scattering layer to the ones without, i.e., the spectral enhancement factor, is presented in Figure 4(b). The maximum enhancement factor and the wavelength at which the maximum enhancement is observed both increase with ETL thickness. For an ETL thickness of 125 nm, the spectral irradiance is increased by up to a factor of 2.9 (at a wavelength of 640 nm). We attribute this effect to the extraction of waveguided modes by the NPSL.

In addition to the improved light outcoupling, the NPSL has two further positive effects: Compared to the reference devices, the shift in color with viewing angle is strongly reduced (Figure 5(a)). For the 80 nm ETL device, the change in CIE between 0° and 75° emission angle is reduced from $\Delta(x,y) = (0.065,0.046)$ for the device without NPSL to $\Delta(x,y) = (0.013,0.004)$ in the device comprising the NPSL.

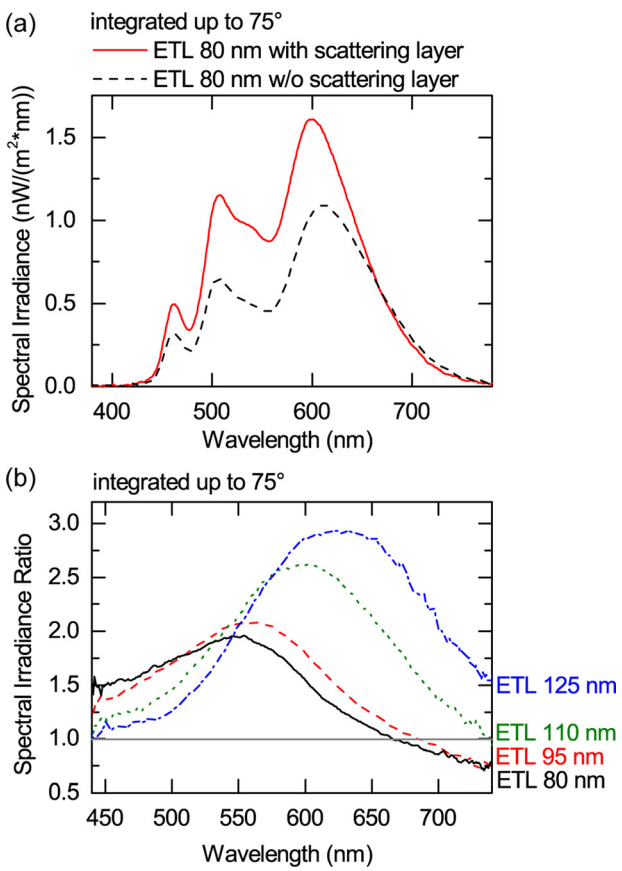

FIG. 4. (a) Angle-integrated total spectral irradiance of white top-emitting OLEDs with (solid line) and without (dashed line) scattering layer. (b) Total spectral irradiance ratio (angle-integrated) for different electron transport layer thicknesses.

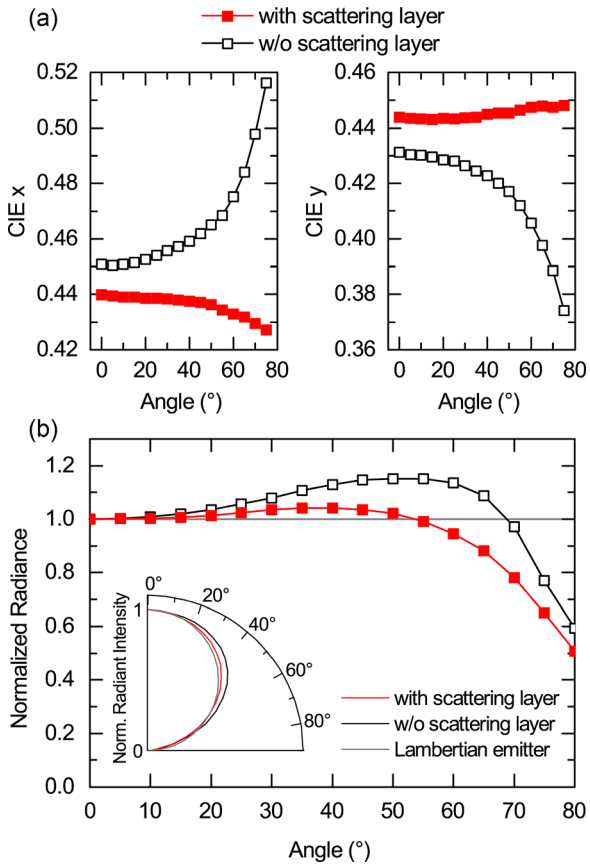

FIG. 5. (a) Change in CIE coordinates with viewing angle for OLEDs with and without scattering layer (ETL thickness, 80 nm). (b) Change in normalized radiance with viewing angle for OLEDs with and without scattering layer (ETL thickness, 80 nm). Dotted line represents the behavior of a Lambertian emitter. The inset shows the same data in a polar coordinate representation.

In addition, the angular distribution of the emission intensity is considerably closer to the ideal Lambertian profile if the NSPL is applied (Figure 5(b)).

In conclusion, we have presented a simple process based on an orthogonal solvent to deposit a NPSL directly on top of small molecule white top-emitting OLEDs without affecting the electrical performance of the device. The homogenous scattering layer improves light outcoupling and increases the efficiency of an already optically optimized white top-emitting OLED by a factor of 1.6. In addition to the efficiency enhancement, the NPSL also increases the color stability under different viewing angles. The concept of using orthogonal HFE solvents to deposit a NPSL directly on top of a top-emitting OLED is compatible with a range of deposition processes, including spray coating and printing, which are cost-effective, fast, reproducible, and involve no additional heating steps. It therefore promises to scale well to large areas and may very well be applicable for industrial processing. In the future, further optimization steps (e.g., regarding size and concentration of the TiO_2 particles) may improve outcoupling efficiency even further. In addition, the NPSL could be combined with internal scattering approaches such as periodic gratings to maximize the outcoupling efficiency.[8]

The authors are grateful to Novaled GmbH (Dresden) for financial support and material supply. M. C. Gather acknowledges financial support from the Scottish Founding Council through SUPA. Hans Kleemann is acknowledged for advice on orthogonal photoresist. T. Schaefer acknowledges Christoph Sachse and Franz Selzer for an introduction to dip-coating. Matthias Böhm and Fabian Patrovsky are acknowledged for providing the dip-coater. The authors are grateful to Tobias Mönch for the AFM measurements.

[1]N. C. Greenham, R. H. Friend, and D. D. C. Bradley, Adv. Mater. **6**, 491 (1994).
[2]G. Gu, D. Z. Garbuzov, P. E. Burrows, S. Venkatesh, S. R. Forrest, and M. E. Thompson, Opt. Lett. **22**, 396 (1997).
[3]W. Brütting, J. Frischeisen, T. D. Schmidt, B. J. Scholz, and C. Mayr, Phys. Status Solidi A **210**, 44 (2013).
[4]S. Reineke, F. Lindner, G. Schwartz, N. Seidler, K. Walzer, B. Lüssem, and K. Leo, Nature **459**, 234 (2009).
[5]S. Möller and S. R. Forrest, J. Appl. Phys. **91**, 3324 (2002).
[6]Y. Sun and S. R. Forrest, Nat. Photonics **2**, 483 (2008).
[7]H.-W. Chang, J. Lee, S. Hofmann, Y. H. Kim, L. Müller-Meskamp, B. Lüssem, C.-C. Wu, K. Leo, and M. C. Gather, J. Appl. Phys. **113**, 204502 (2013).
[8]T. Schwab, C. Fuchs, R. Scholz, A. Zakhidov, K. Leo, and M. C. Gather, Opt. Express **22**, 7524 (2014).
[9]S. Hofmann, M. Thomschke, B. Lüssem, and K. Leo, Opt. Express **19**, A1250 (2011).
[10]Q. Huang, K. Walzer, M. Pfeiffer, V. Lyssenko, G. He, and K. Leo, Appl. Phys. Lett. **88**, 113515 (2006).
[11]R. Meerheim, M. Furno, S. Hofmann, B. Lüssem, and K. Leo, Appl. Phys. Lett. **97**, 253305 (2010).
[12]S. Hofmann, M. Thomschke, P. Freitag, M. Furno, B. Lüssem, and K. Leo, Appl. Phys. Lett. **97**, 253308 (2010).
[13]M. Thomschke, S. Reineke, B. Lüssem, and K. Leo, Nano Lett. **12**, 424 (2012).
[14]J. Kim, J. Lee, C. Moon, K. Kim, and J. Kim, Org. Electron. **17**, 115 (2015).
[15]M. C. Gather and S. Reineke, J. Photonics Energy **5**, 57607 (2015).
[16]S. Reineke, M. Thomschke, B. Lüssem, and K. Leo, Rev. Mod. Phys. **85**, 1245 (2013).
[17]A. A. Zakhidov, J. K. Lee, H. H. Fong, J. A. DeFranco, M. Chatzichristidi, P. G. Taylor, C. K. Ober, and G. G. Malliaras, Adv. Mater. **20**, 3481 (2008).
[18]P. G. Taylor, J. K. Lee, A. A. Zakhidov, M. Chatzichristidi, H. H. Fong, J. A. DeFranco, G. G. Malliaras, and C. K. Ober, Adv. Mater. **21**, 2314 (2009).
[19]P. G. Taylor, J.-K. Lee, A. A. Zakhidov, H. S. Hwang, J. A. DeFranco, H. H. Fong, M. Chatzichristidi, E. Murotani, G. G. Malliaras, and C. K. Ober, Proc. SPIE **7639**, 76390Z (2010).
[20]A. A. Zakhidov, B. Lüssem, K. Leo, and J. DeFranco, Dig. Tech. Pap. - Soc. Inf. Disp. Int. Symp. **42**, 1740 (2011).
[21]X. Gong, D. Moses, G. C. Bazan, and A. J. Heeger, Adv. Mater. **17**, 2053 (2005).
[22]T. Kinkeldei, C. Zysset, N. Münzenrieder, L. Petti, and G. Tröster, Sensors **12**, 13681 (2012).
[23]J. H. Beck, R. A. Barton, M. P. Cox, K. Alexandrou, N. Petrone, G. Olivieri, S. Yang, J. Hone, and I. Kymissis, Nano Lett. **15**, 2555 (2015).
[24]S. Krotkus, F. Ventsch, D. Kasemann, A. A. Zakhidov, S. Hofmann, K. Leo, and M. C. Gather, Adv. Opt. Mater. **2**, 1043 (2014).
[25]T. Schwab, S. Schubert, S. Hofmann, M. Fröbel, C. Fuchs, M. Thomschke, L. Müller-Meskamp, K. Leo, and M. C. Gather, Adv. Opt. Mater. **1**, 707 (2013).
[26]See http://omlc.org/software/mie/ for the implementation of the MIE scatting model used here.
[27]See supplementary material at http://dx.doi.org/10.1063/1.4937004 for Figs S1–S3, illustrating reproducibility, leakage current, and detailed emission spectra, respectively.
[28]T. Schwab, S. Schubert, L. Müller-Meskamp, K. Leo, and M. C. Gather, Adv. Opt. Mater. **1**, 921 (2013).
[29]M. Furno, R. Meerheim, S. Hofmann, B. Lüssem, and K. Leo, Phys. Rev. B **85**, 115205 (2012).